JOURNAL OF GEOPHYSICAL RESEARCH, VOL. 111, D22310, doi:10.1029/2005JD007022, 2006

Tropospheric and stratospheric BrO columns over Arrival Heights, Antarctica, 2002

R. Schofield,[1,2,3] P. V. Johnston,[1] A. Thomas,[1] K. Kreher,[1] B. J. Connor,[1] S. Wood,[1] D. Shooter,[2] M. P. Chipperfield,[4] A. Richter,[5] R. von Glasow,[6] and C. D. Rodgers[7]

Received 13 January 2006; revised 13 June 2006; accepted 27 July 2006; published 28 November 2006.

[1] Spectroscopic measurements of BrO using direct sun and zenith sky viewing geometries are combined in an optimal estimation retrieval algorithm to obtain tropospheric and stratospheric columns of BrO. Twenty-two twilight periods are investigated over Arrival Heights, Antarctica (77.8°S, 166.7°E) during the polar spring period of 2002. This paper presents the first tropospheric and stratospheric BrO column retrievals from UV-visible ground-based measurements for a polar location. A direct comparison is made between stratospheric columns retrieved at 80°, 84°, and 88° solar zenith angles (SZA) from the spectroscopic measurements and those calculated by the SLIMCAT three-dimensional chemical transport model. The ground-based column BrO observations are consistent with a SLIMCAT stratospheric Br_y loading of 21.2 parts per trillion at 20 km. SLIMCAT reproduces the observed sunrise column BrO increase but does not match the sunset observations, which display less variation. The significant warming of the Antarctic polar stratosphere in 2002 led to highly variable stratospheric columns being observed. The observed column BrO decreased with the transition from vortex to extravortex air on 21 September but did not change much following the return of the vortex on 12 October. For the tropospheric column, an almost normal distribution consistent with a "background" of $0.3 \pm 0.3 \times 10^{13}$ molecules cm^{-2} is observed from the ground (80°, 84°, and 88° for both sunrise and sunset). A statistically significant "bromine explosion" event (at the 2σ level) was detected at the end of October with a tropospheric column of $1.8 \pm 0.1 \times 10^{13}$ molecules cm^{-2}. The measured tropospheric columns are compared with the tropospheric Model of Atmospheric Transport and Chemistry–Max Planck Institute for Chemistry version model. The tropospheric BrO sunrise column observations can only be explained with an additional bromine source other than decomposition of CH_3Br and downward transport of long-lived bromine from the stratosphere. A comparison with the spaceborne Global Ozone Monitoring Experiment (GOME) found the total columns observed from the ground to be 16–25% smaller than the total columns observed by GOME for SZAs between 80° and 88°.

Citation: Schofield, R., et al. (2006), Tropospheric and stratospheric BrO columns over Arrival Heights, Antarctica, 2002, *J. Geophys. Res.*, *111*, D22310, doi:10.1029/2005JD007022.

1. Introduction

[2] In the stratosphere catalytic ozone destruction cycles involving bromine are thought to account for ~40% of the ozone loss over Antarctica [*Lee et al.*, 2002]. While this ozone loss is limited by the heterogeneous release of chlorine from its reservoir species on polar stratospheric clouds (PSCs), bromine continues to destroy ozone in the absence of PSCs via the hydrolysis of $BrONO_2$ on cold stratospheric aerosol [*Solomon*, 1999; *Danilin et al.*, 1996; *Lee et al.*, 2002]. At midlatitudes between 30–60°S catalytic ozone destruction involving bromine accounts for about a quarter of the observed ozone losses during winter and spring [*Lee et al.*, 2002].

[3] The polar spring of 2002 in the Antarctic was an unusual year with the polar vortex splitting in two and the remaining vortex becoming weaker, resulting in reduced

[1]National Institute of Water and Atmospheric Research, Central Otago, New Zealand.
[2]School of Geography and Environmental Science, University of Auckland, Auckland, New Zealand.
[3]Now at Chemical Sciences Division, Earth Systems Research Laboratory, National Oceanic and Atmospheric Administration, Boulder, Colorado, USA.
[4]Institute for Atmospheric Science, School of Earth and Environment, University of Leeds, Leeds, UK.
[5]Institute of Environmental Physics, University of Bremen, Bremen, Germany.
[6]Institute of Environmental Physics, University of Heidelberg, Heidelberg, Germany.
[7]Atmospheric, Oceanic and Planetary Physics, Department of Physics, University of Oxford, Oxford, UK.

0148-0227/06/2005JD007022$09.00

stratospheric ozone loss relative to previous years [*Hoppel et al.*, 2003; *Allen et al.*, 2003]. The early polar vortex split due to the unprecedented stratospheric warming provided a unique opportunity to study air masses both inside and outside the polar vortex from the ground at Arrival Heights (77.8°S, 166.7°E) early in the polar spring.

[4] Long-lived bromine source gases account for a stratospheric bromine loading of ~15 parts per trillion by volume (pptv) [*World Meteorological Organization* (*WMO*), 2003]. Combined observational and chemical modeling studies from 1995 to present indicate that the stratospheric bromine loading is between 18 ± 3 and 21.5 ± 3 pptv [*Fish et al.*, 1995; *Pfeilsticker et al.*, 2000; *Sinnhuber et al.*, 2002, 2005; *Schofield et al.*, 2004b; *Salawitch et al.*, 2005]. Transport of short-lived tropospheric bromine species to the stratosphere is required to be included within models to explain this shortfall in the total stratospheric bromine budget.

[5] In the polar regions the role of BrO causing almost complete boundary layer ozone loss has been well documented in the Arctic [*Barrie et al.*, 1988; *Bottenheim et al.*, 1990; *Solberg et al.*, 1996; *Tuckermann et al.*, 1997; *Miller et al.*, 1997; *Oltmans et al.*, 1998] and Antarctic [*Kreher et al.*, 1997; *Frieß et al.*, 2005]. The linkage of these high-BrO events and increased mercury deposition (thus increased mercury levels in the polar biosphere) has major health implications for the polar regions [*Schroeder and Munthe*, 1998]. The exact mechanism for the release of bromine is currently not fully understood. Proposed mechanisms include the autocatalytic release of bromine from sea salt either from accumulation on the snowpack over the polar winter with subsequent snow processing [*Tang and McConnell*, 1996], or from sea salt aerosol processing [*Simpson et al.*, 2005]. There is increasing evidence for the involvement of frost flowers [*Kaleschke et al.*, 2004], however, the exact role of open leads and frost flower involvement in the process is unknown [*Simpson et al.*, 2005].

[6] The ability to differentiate tropospheric and stratospheric trace gas species is vital because of the very different processes that occur in these regions, and this is especially true for BrO in the polar regions. The Umkehr method of retrieving the vertical distribution of ozone from ground-based spectroscopy was originally described by *Mateer and Duetsch* [1964] and *Ramanathan and Dave* [1957] and more recently applied in advanced retrievals [e.g., *Petropavlovskikh et al.*, 2005]. A similar technique using observations at different sun angles for ground-based stratospheric profiling was pioneered by *Brewer et al.* [1973], *Noxon* [1975], and *McKenzie et al.* [1991] for NO_2. Recent work by *Preston et al.* [1997] and *Hendrick et al.* [2004] have implemented the formal optimal estimation method of *Rodgers* [2000] in stratospheric profile retrievals of NO_2 from ground-based zenith sky spectroscopy. Tropospheric and stratospheric BrO column retrievals have been performed by *Schofield et al.* [2004a] for the midlatitude site of Lauder, New Zealand. BrO in the boundary layer has been retrieved using MAXDOAS with a geometric interpretation by *Hönninger and Platt* [2002]. The use of O_4 to constrain the tropospheric path will enable more accurate boundary layer profiling from MAXDOAS in the future [*Wagner et al.*, 2004; *Sinreich et al.*, 2005]. This paper presents the first tropospheric and stratospheric BrO column retrieval from UV-visible ground-based measurements for a polar location.

2. Ground-Based Spectroscopic Measurements

[7] Spectroscopic measurements are made at Arrival Heights, Antarctica (77.8°S, 166.7°E) located at an altitude of 185 m above the sea ice on Ross Island, at the edge of the Ross Sea ice shelf. Arrival Heights is one of the primary measurement sites that makes up the Network for the Detection of Stratospheric Change (NDSC), now the Network for the Detection of Atmospheric Composition Change (NDACC).

2.1. Instrumentation

[8] Zenith sky measurements were made with an Acton SpectraPro-500 spectrometer (a commercial Czerny Turner monochromator), with a focal length of 500 mm, an aperture ratio of f/6.9 and a field of view of 7°. The detector was a photo diode array cooled to −50°C. The 1200 grooves mm^{-1} grating provides a wavelength coverage of 332–371 nm at a resolution of 0.58 nm and full width half maximum (FWHM) of 15.5 pixels. A detailed description of the spectrometer and nonlinear least squares differential optical absorption spectroscopy (DOAS) method used to derive the zenith sky differential slant column densities (DSCDs) is given by *Kreher et al.* [1997]. Zenith sky measurements were made up to 95° solar zenith angles (SZA) because of the slow change in SZA at this polar latitude. The resultant longer integration times increased the signal to noise, and thus reduced the measurement errors.

[9] The direct sun viewing spectrometer was an Acton 275 (a commercial Czerny Turner spectrometer with spherical mirrors). The detector was a Hamamatsu back thinned charge coupled device (CCD) module with 1044 3.2 mm × 0.024 mm pixels. The detector was cooled to −20°C. The 1200 grooves mm^{-1} grating provides a wavelength coverage of 324–395 nm at a resolution of 0.5 nm and FWHM sampling of about 7 pixels. A complete instrument description and DSCD DOAS derivation is given by *Schofield et al.* [2004b]. The low horizon surrounding the Arrival Heights site allowed direct sun measurements to be made up to 89° SZA.

2.2. DOAS Analysis

[10] DSCD values from both direct sun and zenith sky viewing spectroscopic measurements were evaluated using the well-known DOAS technique (for a review of DOAS see *Platt* [1994]). A ratio of twilight radiance spectra with respect to a noon reference spectrum removes the complicating Fraunhofer lines present in solar radiance measurements. In both the direct sun and zenith sky geometries noon reference spectra were chosen for each day (as close as possible to the local noon, yet still under cloud-free conditions). The range of SZAs sampled by the DSCDs differed between measurement days because of clouds, solar elevation and the topography. The broadband absorption features and the Rayleigh and Mie scattering features that make up the spectral background baseline were removed by fitting low-order polynomials (high-pass filter). A nonlinear least squares fitting procedure was then employed to fit differential cross sections for each absorber, thus determining

their respective absorptions [*Aliwell et al.*, 2002]. The cross sections of O_4 [*Greenblatt et al.*, 1990], O_3 [*Voigt et al.*, 2001] (203 K and 280 K), NO_2 [*Harder et al.*, 1997], OClO [*Kromminga et al.*, 2003], BrO [*Wilmouth et al.*, 1999], Ring (measured) [*Fish and Jones*, 1995; *Solomon et al.*, 1987] and CH_2O [*Meller and Moortgat*, 2000] were fitted to the logarithm of the spectral ratio of the twilight to noon radiances. For the zenith sky DSCDs a fitting window of 344.5–358.5 nm was used. The direct sun DSCDs used a fitting window of 345.8–359.8 nm.

2.3. Measurement Covariance

[11] The covariance matrix of the uncertainties in the measurements $\mathbf{S}_\epsilon$ was constructed by placing the variance arising from one standard deviation of the error from the DOAS spectral fitting along the diagonal of the matrix. The off-diagonal elements are assumed to be zero. The measurement error covariance matrix derived from the DOAS fitting is assumed to incorporate all the errors that are present in determining the DSCDs.

2.4. Column Retrievals

[12] The methodology for retrieving tropospheric and stratospheric columns at a number of SZAs by combining direct sun and zenith sky measurements is described in detail by *Schofield et al.* [2004a]. In brief: the direct sun DSCDs and the zenith sky DSCDs are combined to create the measurement vector $\mathbf{y}$. A radiative transfer model (forward model) calculates the DSCDs for a given series of BrO profiles at different SZA; this is the state vector $\mathbf{x}$. Each element of the matrix of BrO profiles is perturbed and the resultant change in the calculated DSCDs is used to construct the Jacobian or weighting function matrix $\mathbf{K}$. Optimal estimation [*Rodgers*, 2000] is the technique used to invert the measurements $\mathbf{y}$ to give the retrieved state $\hat{\mathbf{x}}$. The prior knowledge of the state $\mathbf{x}_a$, its covariance $\mathbf{S}_a$, the measurements $\mathbf{y}$ and their covariance $\mathbf{S}_\epsilon$ are all included in the inversion to give the solution which is optimal given the constraints of the measurements and a priori knowledge. The equation that is solved for the linear problem is

$$\hat{\mathbf{x}} = \mathbf{x}_a + \mathbf{S}_a\mathbf{K}^T\left(\mathbf{K}\mathbf{S}_a\mathbf{K}^T + \mathbf{S}_\epsilon\right)^{-1}(\mathbf{y} - \mathbf{K}\mathbf{x}_a) \qquad (1)$$

Stratospheric and tropospheric columns are then derived at each SZA by integrating the appropriate altitude range of $\hat{\mathbf{x}}$.

2.4.1. Forward Model

[13] The calculation of the DSCDs for a given set of BrO profiles is conducted by a radiative transfer algorithm. The radiative transfer algorithm is defined with spherical coordinates from 0 to 70 km in discrete atmospheric layers. The effects of refraction, molecular absorption, Rayleigh and Mie scattering were included. Only first-order scattering is included, since multiple scattering is negligible for the DSCDs of BrO for SZA $< 92°$ [*Sinnhuber et al.*, 2002; *Hendrick et al.*, 2006]. The radiative transfer model (forward model) parameters of ozone, temperature and pressure describing the climatology were provided by ozonesonde measurements conducted at McMurdo (4 km from Arrival Heights). The aerosol extinction profile was derived from lidar measurements at McMurdo. For the troposphere, an aerosol extinction profile from the winter climatology of Lauder was assumed (J. B. Liley, personal communication, 2003), derived from backscatter sondes. The NO_2 profile was obtained from SAGE II measurements made on 7 October 2002 for Arrival Heights. The forward model parameters were all found to produce negligible errors in the final retrieved values [*Schofield*, 2003] (see also section 2.4.4). The date 7 October was chosen and these profiles were held constant for all of the retrievals.

[14] A tropopause height of 8.8 km was used for all of the polar column retrievals. This height was derived by considering all of the ozonesonde data (8 flights) available for the spring period of 2002. The effect of different tropopause heights is discussed in section 4.2.

2.4.2. State Vector, A Priori, and A Priori Covariance

[15] The diurnal variation of the vertical distribution of trace gas species of NO_2 and BrO adds complication to the retrieval problem. This has been addressed by *Preston* [1995] and *Hendrick et al.* [2004] by incorporating a photochemical model in the forward modeling of the inversion problem. *Schofield et al.* [2004a, 2004b] simultaneously retrieve the diurnal change in the trace gas distribution directly from the measurements.

[16] Similar to the tropospheric and stratospheric column retrievals performed for the midlatitude site, Lauder [*Schofield et al.*, 2004b], the state vector is composed of BrO profiles at different diurnal stages to account for the strong diurnal variation of BrO. The state vector is constructed from the seven profiles at SZAs of 0°, 80°, 84°, 88°, 90°, 92° and 97°, with each profile from 0 to 70 km in steps of 1 km, thus $\hat{\mathbf{x}}$ is a vector of length 7×71 (with the profiles stacked in ascending order of SZA).

[17] A stationary chemical box model was used to determine the stratospheric a priori set of profiles using SLIMCAT [*Chipperfield*, 1999] chemistry with the most recent update of reaction rates [*Sander et al.*, 2003]. Unlike the midlatitude case where there is a clear decrease in the VCD from 80° SZA, the slower rate of change of SZA in the polar scenario means that seven profiles can be chosen to describe the diurnal change (0°, 80°, 84°, 88°, 90°, 92° and 97° SZA) with the model predicting a decrease in the VCD to occur after 90° for the sunset on 7 October. There is almost no diurnal variation between the 80° and 90° stratospheric profiles. There is however, a rapid decrease in the BrO VCD from 90° to 92°, with almost no BrO present at 97°. Figure 1 shows the a priori profile diurnal variation for Arrival Heights in the spring used for the column retrievals in this work. The a priori 0° tropospheric profile used is based on a winter balloon BrO observation made at Kiruna [*Fitzenberger et al.*, 2000]. The a priori noon profile is assumed to have a peak at $\sim 1 \times 10^{13}$ molecules cm^{-3} at 3 km and decreasing to zero at the tropopause. For the other tropospheric a priori profiles a diurnal decrease similar to the diurnal decrease in the stratosphere was assumed. These tropospheric a priori assumptions are discussed in section 4.2.

[18] An a priori error of 30% of the peak value was assumed in the construction of $\mathbf{S}_a$. The a priori covariance of the Lauder data set [*Schofield et al.*, 2004b] was 50%. The smaller a priori error (larger constraint) was required because of the smaller SZA range of the Arrival Heights measurements, especially at the beginning of the measurement period. The 30% error was sufficient to provide a good

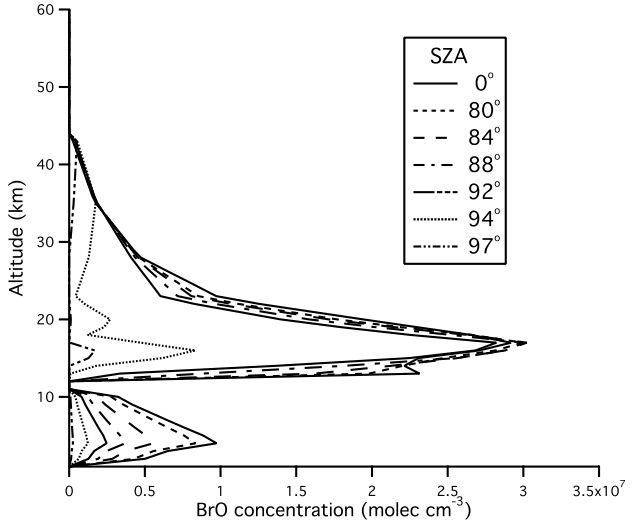

Figure 1. BrO profiles supplied as a priori information in all of the retrievals performed for Arrival Heights.

fit for all of the Arrival Heights measurements without overfitting them.

2.4.3. Characterization

[19] The averaging kernels are the rows of the averaging kernel matrix and describe the smoothing of the true state ($\mathbf{x}$) by the retrieval of each point that makes up the retrieved profile $\hat{\mathbf{x}}$. The averaging kernel matrix is evaluated with the following equation.

$$\mathbf{A} = \frac{\partial \hat{\mathbf{x}}}{\partial \mathbf{x}} = \left(\mathbf{K}^T \mathbf{S}_\epsilon^{-1} \mathbf{K} + \mathbf{S}_a^{-1}\right)^{-1} \mathbf{K}^T \mathbf{S}_\epsilon^{-1} \mathbf{K} \qquad (2)$$

[20] The averaging kernels for the tropospheric and stratospheric columns for each of the seven state profiles were evaluated from $\mathbf{A}$ summing over the relevant altitudes in the state to give tropospheric and stratospheric columns for each of the seven state profiles. The averaging kernels for the retrievals of the 80°, 84° and 88° columns are provided in the auxiliary material.[1]

[21] The averaging kernels for the tropospheric and stratospheric columns for the Arrival Heights retrievals were influenced by the different SZA ranges of the measurements. The tropospheric and stratospheric columns displayed good separation for all days. The stratospheric column for the 88° profile was consistently the least well described column, this being the cause of the large smoothing error for this column. Examples of the column averaging kernels for the DSCD measurements shown in Figure 2 are given in the auxiliary material, along with the retrieved profiles (before being integrated to columns).

[22] The mean Shannon information content [*Rodgers*, 2000] and degrees of freedom for signal, quantities derived from the averaging kernels for each of the columns are displayed in Table 1. The information content describes the reduction in the uncertainty in the state that results from making the measurement. The degrees of freedom for signal describes the number of useful independent pieces of information in the retrieved quantity. Having less than one degree of freedom for signal for the tropospheric columns indicates that these are not as well described by the measurements as the stratospheric columns, and hence have more a priori dependence. The measurements contain the least stratospheric column information for 88° and the most information for 84°. The averaging kernels for the 84° profile retrieval peak at the desired altitudes between ~18–40 km, whereas for the 88° profile retrieval the averaging kernels have a focused peak at ~20 km over the same altitude range.

[23] The information content and degrees of freedom for signal for each of the Arrival Heights retrievals was dependent on the SZA range. Early in the measurement period the retrievals had few or no independent pieces of information about the 80° columns since the sun never reached this SZA. The retrievals toward the end of the measurement period had a much larger SZA range, and with the long integration times, they contained much more information about the 80°, and slightly less about the 88° columns. Because of the longer integration times associated with the polar latitude and the elevation of the Arrival Heights site above the surrounding horizon it was possible to retrieve 88° columns (compared to Lauder where retrieving 87° only was possible). The measurement errors are low because of the longer integration times, and the ability to measure in both geometries to high SZAs.

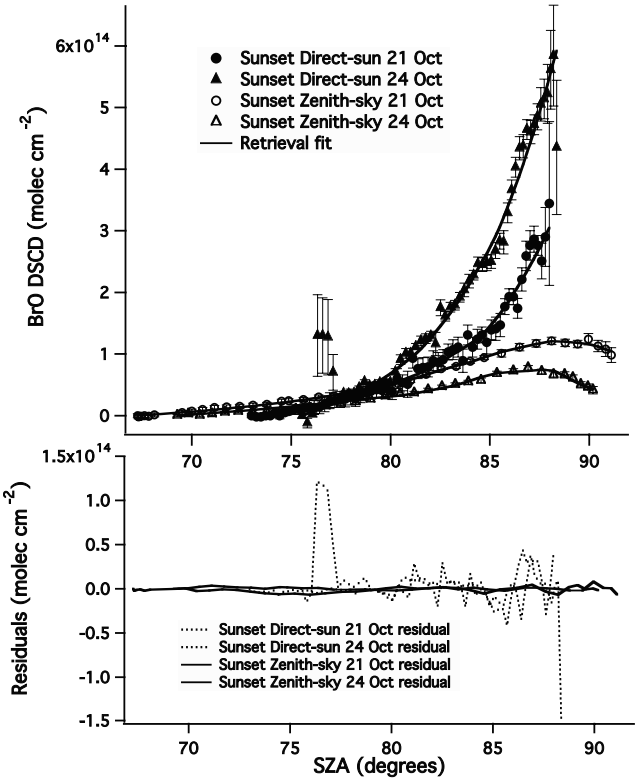

Figure 2. (top) Differential slant column measurements and retrieval fit for days with background (21 October) and high (24 October) tropospheric BrO. (bottom) Residuals for the model fit to the measurement. The high DSCDs in the direct sun at ~77° indicate a cloudy period.

[1] Auxiliary materials are available in the HTML. doi:10.1029/2005JD007022.

Table 1. Retrieved Columns, Errors, Information Content, and Degrees of Freedom for Arrival Heights, 2002

	Tropospheric Column			Stratospheric Column		
	80°	84°	88°	80°	84°	88°
Sunrise (σ)[a,b]	0.70 (0.63)	0.44 (0.21)	0.25 (0.17)	3.05 (0.59)	3.08 (0.45)	2.66 (0.27)
Sunset (σ)[a,b]	0.15 (0.23)	0.24 (0.15)	0.32 (0.22)	2.52 (0.58)	2.43 (0.45)	2.51 (0.30)
High BrO (σ)[a,b]	1.65 (0.12)	1.88 (0.12)	1.60 (0.12)	2.49 (0.59)	3.02 (0.66)	3.09 (0.35)
Total retrieval error[b]	0.17	0.13	0.14	0.23	0.28	0.51
Temperature error[b]	0.02	0.01	0.005	0.03	0.01	0.01
Information content[c]	0.4	0.6	0.6	2.1	2.1	1.2
Degrees of freedom[d]	0.5	0.7	0.7	1.7	2.1	1.5

[a]The column values are mean values over observation days for sunrise (8 twilight days (23 September to 20 October)), sunset (12 days (10 September to 21 October)), and high tropospheric BrO (2 days (24–25 October)), with the standard deviation given in parentheses.
[b]Columns and errors are in units of $\times 10^{13}$ molecules cm^{-2}.
[c]Information content is in bit units (base 2).
[d]Degrees of freedom is the number of independent pieces of information.

2.4.4. Retrieval Error Analysis

[24] An error analysis was conducted which applies to all 22 of the twilight measurements at Arrival Heights. The total retrieval error is defined here as the sum of the retrieval noise, smoothing error and forward model parameter error. The forward model parameters of temperature, surface pressure, ozone and aerosol extinction were investigated for their contribution to the total retrieval errors. The variability in these quantities all produced a negligible contribution to the total retrieval error. The total retrieval error and the error due to the temperature profile (largest forward model parameter error) in the retrieved quantities are also given in Table 1.

2.4.5. Retrieval Fit to the Measurements

[25] Figure 2 displays DSCD measurements ($\mathbf{y}$) for a day of background tropospheric BrO and a day of high tropospheric BrO, with the retrieval fit ($\hat{\mathbf{y}}$). The retrieval residuals $\mathbf{y} - \hat{\mathbf{y}}$ are also displayed. The mean residuals over the data set allow systematic errors to be identified in either the forward model, DSCD determination or in the measured DSCDs. The direct sun residuals illustrate that some systematic errors were present in the direct sun viewing geometry. A contributing factor to the higher direct sun residuals could be the necessary filter changes and problems in fitting O_4 in the DSCD determination. O_4 becomes increasingly important with longer tropospheric paths at high SZA. The systematic errors between 70° and 90° represent about 10% of the absolute direct sun DSCDs.

[26] The mean residuals for the retrieval fit of the zenith sky measurements indicated that the measurements were systematically lower than the forward model for large SZA. This possibly indicates that the forward model is no longer a good approximation to the true atmospheric radiative transfer at large SZA and that multiple scattering becomes important at SZA greater than 92° for the calculation of BrO zenith sky DSCDs [*Sinnhuber et al.*, 2002; *Hendrick et al.*, 2006]. These errors in the highest SZA (>90°) for the zenith sky DSCDs correspond to about 15%.

3. Chemical Model and Global Ozone Monitoring Experiment (GOME) Descriptions

[27] The descriptions of the Model of Atmospheric Transport and Chemistry–Max Planck Institute for Chemistry version (MATCH-MPIC) used to calculate tropospheric BrO and the stratospheric BrO columns derived from three-dimensional (3-D) SLIMCAT model are given in this section. Measurements made by the Global Ozone Monitoring Experiment (GOME) satellite experiment are also discussed within this section.

3.1. Stratospheric BrO Modeling: SLIMCAT

[28] In this study we have used output from a simulation of the 3-D SLIMCAT off-line chemical transport model (CTM) [*Chipperfield*, 1999]. The model has a detailed treatment of gas phase and heterogeneous stratospheric chemistry. The model temperatures and horizontal winds are specified from meteorological analyses and the vertical transport in the stratosphere is diagnosed from radiative heating rates. In the stratosphere the model uses an isentropic coordinate and this has recently been extended down to the surface using hybrid $\sigma - \theta$ levels. The principal advantage of this new version of SLIMCAT is that the model boundary has been removed from the tropopause region [*Chipperfield*, 2006].

[29] In the run used here the model was integrated with a horizontal resolution of 7.5° × 7.5° and 24 levels extending from the surface to about 55 km. The model was forced by European Centre for Medium Range Weather Forecasts (ECMWF) analyses and the simulation started 1/1/1977. The model halogen loading was specified (as a mixing ratio in the surface layer) from observed tropospheric CH_3Br and halon loadings [e.g., *WMO*, 2003] with an additional 6 pptv contribution assumed from short-lived bromine sources. Accordingly, the model stratospheric bromine loading around 2002 was about 21.2 pptv. Output was saved at 0 UT every 2 days and linearly interpolated to the location of Arrival Heights from the nearest 4 grid points at each model output time. A 1-D column model (with the identical chemistry to the 3-D model) was then used to reconstruct the diurnal cycle for comparison with the observations.

[30] The tropopause was defined to be the lower altitude of the layer for which the decrease in temperature with altitude was less than 2°C per km above 500 hPa. The SLIMCAT model layers in the run used here have a thickness of about 4 km in the tropopause region thus the tropopause was calculated to be about 8–9 km, ensuring that part of the stratospheric BrO amount was not partitioned into the tropospheric column.

3.2. Tropospheric BrO Modeling: MATCH-MPIC

[31] Match Tropospheric BrO columns are calculated using the off-line 3-D tropospheric chemical transport model MATCH-MPIC [*von Kuhlmann et al.*, 2003] which has been extended to include bromine gas phase and heterogeneous reactions on aerosol particles [*von Glasow et al.*, 2004]. It includes 66 species and 163 chemical reactions. The model runs used here for comparison with the observational data are described in detail by *von Glasow et al.* [2004]. The global sources for reactive bromine for the (free) troposphere include release of bromine from sea salt aerosol and upward transport, breakdown of organic precursors, upward transport of bromine from polar boundary layer ozone depletion events, downward transport of inorganic bromine from the stratosphere, biomass burning, and volcanoes, but they are still quantitatively ill constrained. In order to cover several possible source scenarios, model runs with a stronger source in high latitudes (case ''high lat''), or the tropics (case ''tropics''), as well as only downward flux of inorganic bromine (long-lived sources only, $Br_y \sim 15$ ppt) from the stratosphere and breakdown of CH_3Br (case ''strat'') are used here for comparisons with the data. For details of the different scenarios and the source strengths see *von Glasow et al.* [2004]. As the purpose of the study by *von Glasow et al.* [2004] was exploratory in nature, a coarse spatial resolution of about 11.3° by 11.3° was used, the grid cell encompassing Arrival Heights includes the region 76.2°S–90°S, 163.1°E–174.4°E. The model time step is 30 minutes and the model output is routinely saved as weekly averages (7 days, 24 hours average value). The tropopause is defined according to the standard WMO lapse rate definition. The meteorology used to force the model for this comparison is from 1998, thus the comparison is more of a ''climatological'' estimate and not specific for 2002.

3.3. GOME

[32] GOME is one of the experiments on the ERS-2 satellite, which was launched in April 1995 [*Burrows et al.*, 1999]. GOME is a nadir viewing experiment with a footprint of 40×320 km^2 and ERS-2 covers the whole Earth in 3 days. The ERS-2 overpasses within 200 km of Arrival Heights were used for this comparative work (10 September to 21 October). At polar latitudes the overpass time for the ERS-2 satellite coincides with large SZAs at the beginning of the polar spring and overpasses within 200 km of Arrival Heights are seen almost daily.

[33] The GOME BrO columns were retrieved using the settings as described by *Richter et al.* [2002]. Briefly, the fitting window 344.7–359 nm is used and BrO, ozone (221 K and a temperature dependence term), NO_2, O_4, Ring, undersampling correction, offset and slope and a cubic polynomial are included in the fit. BrO vertical columns are retrieved using air mass factors calculated at 351.85 nm using the radiative transfer model SCIATRAN including maritime aerosol, with a ground albedo of 0.9 [*Richter et al.*, 1998]. The profile shape was assumed to be the same as retrieved from the ground-based measurements with the exception of the days with enhanced BrO in the boundary layer, where background tropospheric values were assumed.

[34] While GOME observations are total column measurements, the sensitivity to the stratosphere and troposphere change over the time period studied here. On 17 September (at 90° SZA), the measurements are nearly insensitive to the boundary layer, while at the end of the time series at 75° SZA, there is a factor of two difference in sensitivity between the surface and 20 km altitude.

4. Results: Retrieved Columns for BrO Over Arrival Heights

[35] Table 1 gives the variance-weighted mean columns over all of the sunrise and sunset column retrievals excluding the high tropospheric BrO days of 24 and 25 October for Arrival Heights. The values in parentheses are the standard deviations of these means, indicating the atmospheric variability in the retrieved columns. The two high tropospheric BrO twilight retrievals are combined and tabulated separately from the other days. The stratospheric column retrievals for the background and high-BrO retrievals are within their respective errors. The variance-weighted mean stratospheric BrO columns over Arrival Heights are similar to the midlatitude 80° and 84° columns retrieved for winter over the midlatitude site of Lauder [*Schofield et al.*, 2004b].

4.1. Stratospheric and Total Columns

[36] Over the measurement period, nine sunrise and thirteen sunset clear-sky twilight periods were examined (this being limited by the number of clear-sky twilights available between 10 September and 25 October). Measurements at the beginning and end of the measurement period were the only ones made while Arrival Heights was under the polar vortex.

[37] The stratospheric BrO columns retrieved from the combined ground-based spectroscopic measurements over the measurement period at Arrival Heights are displayed in Figure 3 along with the SLIMCAT model results for 80°, 84° and 88° for sunrise and sunset. The shaded parts indicate when Arrival Heights was under the stratospheric polar vortex as determined from Total Ozone Mapping Spectrometer measurements [*Heath et al.*, 1975]. During most years Arrival Heights would be under the polar vortex for the entirety of the spring period. However, 2002 was an exception and the vortex split meant that Arrival Heights was outside the vortex between 22 September and 11 October. The retrieved and modeled stratospheric BrO columns were highly variable because of the increased dynamic activity in 2002, as well as the polar spring already being a very changeable time with respect to photochemistry. The overall agreement between the observed columns and the SLIMCAT model with ~21.2 ppt Br_y is good, with the exception of the disturbed vortex conditions around 21 September.

[38] There is only a slight difference in the stratospheric BrO columns (measured and modeled) when inside or outside the vortex (compared with chlorine), consistent with the partitioning of reactive bromine favoring the radical species BrO in the gas phase (BrO/Br_y ratios range between 0.3 and 0.6 for 10–20 km, similar to the bromine partitioning seen in the Arctic polar lower stratosphere by *Avallone and Toohey* [2001]). Inside the vortex (7–20 September) there was more Br_y in the lower stratosphere (above 12 km) consistent with increased downwelling compared to the days outside the vortex after 21 September. For the vortex

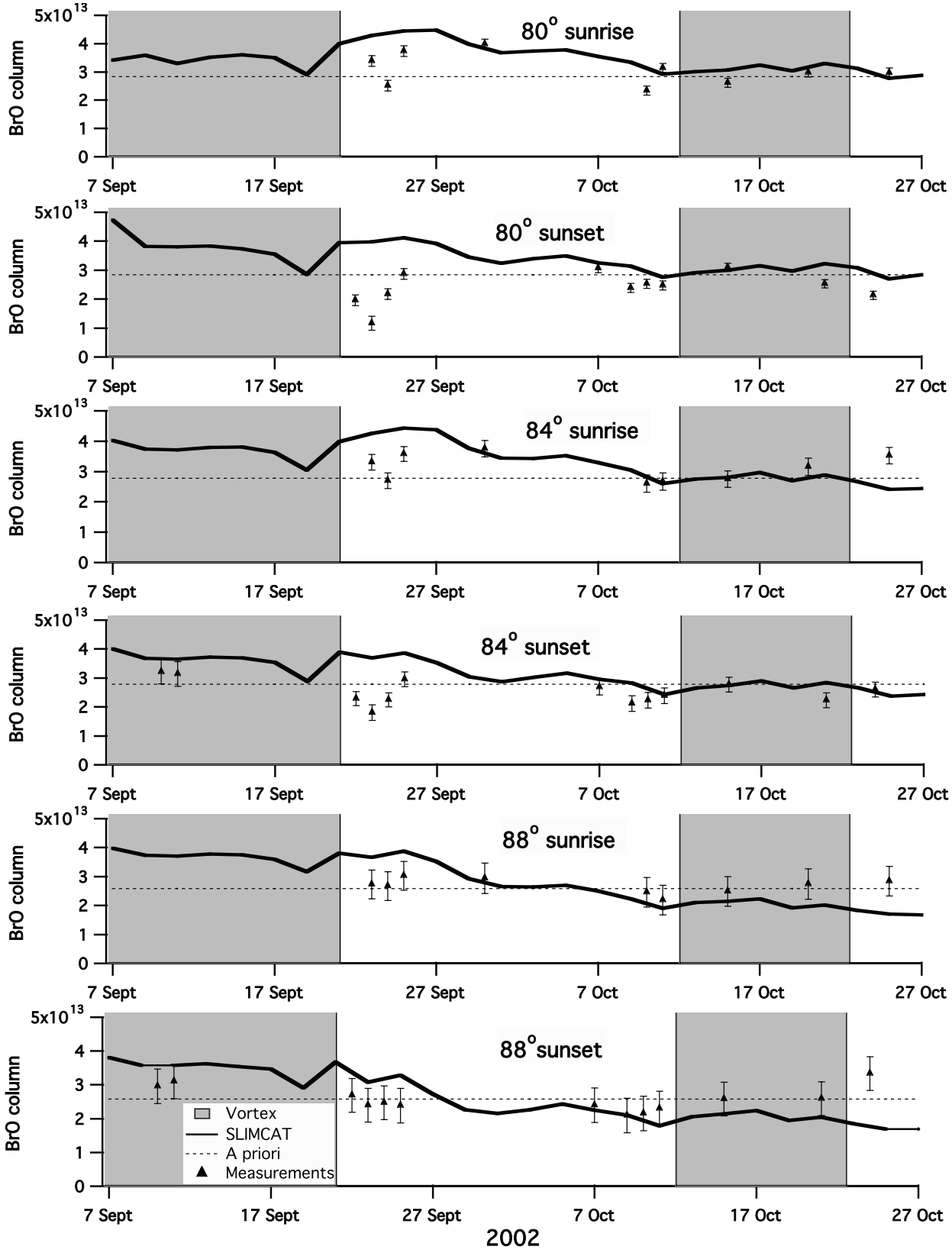

Figure 3. Stratospheric columns (molecules cm^{-2}) of BrO measured at Arrival Heights (solid triangles) and those calculated by SLIMCAT (solid black lines). The sunrise and sunset columns retrieved for 80° are given by the top two plots, for 84° by the middle two plots, and for 88° by the bottom two plots. The error bars given on the observations are the errors arising from the retrieval of the column (smoothing and propagated DSCD error). The shaded portions indicate when Arrival Heights was under the polar vortex. The dashed line gives the a priori column used for all the retrievals.

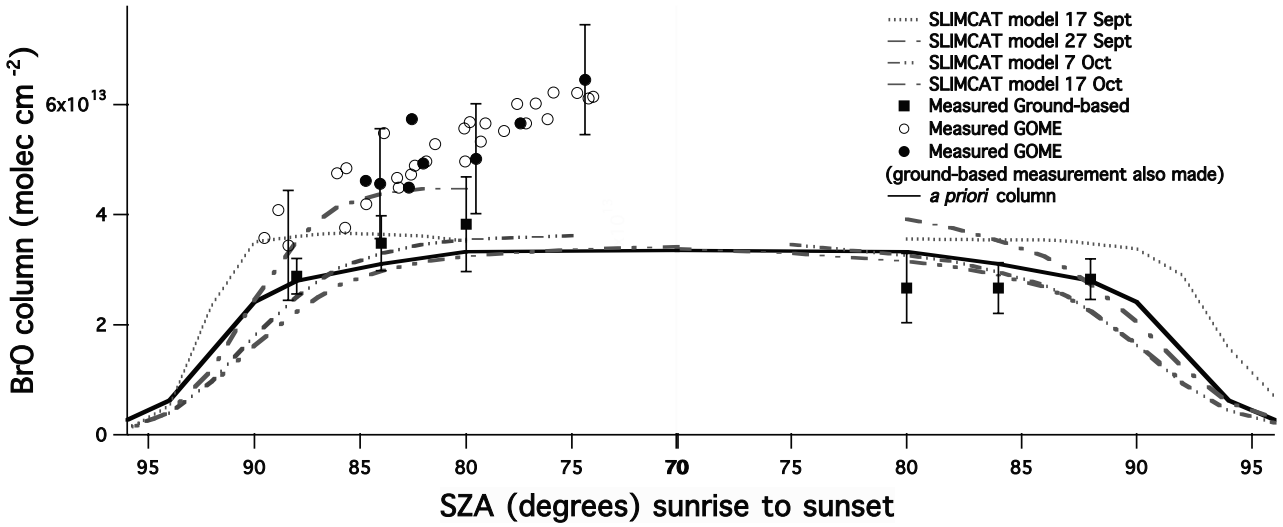

Figure 4. Diurnal variation (with SZA) of the total BrO column. The mean ground-based total columns are displayed with the filled squares, with the error bars representing one standard deviation of the retrieved columns (illustrating the range of retrieved columns consistent with atmospheric variability). The GOME total columns are shown with open circles, and solid circles indicate a GOME measurement when ground-based measurements were also made. The calculated total columns from SLIMCAT are displayed for 17 September, 27 September, 7 October, and 17 October. The a priori total column is displayed with the solid line.

to extravortex transition seen on 21 September the temperatures driving the SLIMCAT results changed from 196 to 230 K and the ozone increased from 1 ppm to 2 ppm at 15 km. The BrO/Br_y partitioning at 15 km changed from 0.45 to 0.55. The days just after 21 September when the vortex was highly disturbed is the period of the worst agreement between observations and the model, most probably due to the low resolution of the model (7.5° × 7.5°) compared to the localized Arrival Heights columns.

[39] The transition from extravortex to vortex air on 12 October was accompanied by a much less dramatic change in SLIMCAT Br_y (decrease of ~1 ppt below 13 km and increase of ~1 ppt between 13 and 20 km), temperature (220 K to 208 K at 15 km, though larger above) and ozone (decrease by ~0.5 ppm at 15–20 km, though the depletion above ~22 km was severe within the late spring vortex). The result on the SLIMCAT modeled BrO columns was to shift the BrO peak up slightly, but not really change the BrO stratospheric column as significantly as predicted for the 21 September vortex transition. The ground-based measured and the SLIMCAT modeled columns for the 12 October transition are in very good agreement overall.

[40] The sunrise columns calculated by SLIMCAT and those retrieved were larger than the sunset columns (refer to Table 1 and also Figures 1 and 4 for this diurnal variation). This is consistent with the enhanced release from the morning BrCl reservoir and also the extended time spent at each SZA at this high-latitude site [*Fish et al.*, 1995]. However, the cause of this asymmetry can vary between in-vortex air extravortex air. Inside the springtime polar vortex, under conditions of chlorine activation, BrCl is produced through a minor channel of the reaction of BrO + ClO. As NO_x levels are low, BrCl is the dominant nighttime reservoir. As ClO at night is in the reservoir form of Cl_2O_2, which is slower to photolyze than BrCl, sunrise levels of BrCl can be suppressed because there is less ClO for reaction with BrO. Under extra vortex, midlatitude conditions $BrONO_2$ will be formed as a significant nighttime reservoir. At night $BrONO_2$ undergoes heterogeneous conversion (hydrolysis) to HOBr, and at colder temperatures typical of higher latitudes, HOBr further reacts via the heterogeneous reaction with HCl to BrCl. BrCl is photolyzed more rapidly than $BrONO_2$ and HOBr leading to enhanced sunrise BrO by this process. The observations are therefore consistent with either or both of these processes occurring, depending on the type of air mass sampled.

[41] Figure 4 displays the mean ground-based total columns, the GOME total columns and the calculated SLIMCAT model total columns. Total columns where auxiliary measurements indicated high surface BrO were excluded from this comparison. SLIMCAT columns are representative mainly of the stratospheric column and these demonstrate how variable the stratosphere was over this measurement period. The diurnal variation of the observed sunrise columns is modeled well, but the sunset column variation modeled by SLIMCAT generally predicts higher 80° BrO columns with a faster loss of BrO into reservoir species, than is observed. Both the vortex and extravortex columns are combined to calculate the mean observed columns for sunrise and sunset displayed in Figure 4. The difference in temperature inside and outside of the polar vortex leading to slightly different diurnal variation, as supported by the very different SLIMCAT columns, can explain some of this discrepancy. However, overall the observed lack of change in the sunset columns is not captured by the SLIMCAT model.

[42] The total columns observed by GOME over all days are also displayed in Figure 4 (open circles). The solid circles are the GOME measurements on clear-sky days when a morning direct sun ground-based observation was

Table 2. Mean Tropospheric Columns and Standard Deviation Retrieved for Different Tropopause Heights and A Priori Assumptions[a]

Tropopause, km	80° Sunrise Trop. Col., $\times 10^{13}$ molecules cm^{-2}	80° A Priori Trop. Col., $\times 10^{13}$ molecules cm^{-2}	Mean Trop. Col., $\times 10^{13}$ molecules cm^{-2}
7.0	0.63 (0.57)	0.40	
8.8	**0.70 (0.63)**	**0.44**	**0.33 (0.32)**
10.0	0.79 (0.73)	0.49	
15.0	1.66 (0.89)	1.29	
8.8	0.92 (0.63)	0.88	0.46 (0.35)
8.8	1.13 (0.63)	1.33	0.58 (0.41)

[a]Tropopause heights of 7–10 km were tested as this represents the variability in the tropopause height over the measurement period. Here 15 km is also calculated to enable comparison with the recent work of *Sinnhuber et al.* [2005]. The effect of doubling and tripling the a priori tropospheric profiles (0–10 km) (Figure 1) is given in the bottom section of the table. The 80° column is most sensitive to the a priori assumption (see Table 1, 0.5 degrees of freedom). The mean tropospheric column over all tropospheric column retrievals (80°, 84°, and 88° sunrise and sunset) increases to $0.58 \pm 0.41 \times 10^{13}$ molecules cm^{-2} if a tropospheric profile three times that in Figure 1 is assumed a priori.

also made. It is important to note that the high-SZA GOME measurements are for days early in the measurement period, whereas the lower SZA GOME measurements represent measurements made at the end of the measurement period. The error bars on the GOME columns represent the estimated error of 1×10^{13} molecules cm^{-2}, a conservative estimate of the error of the GOME column retrievals. The total columns observed by GOME are generally higher than the ground-based column amounts even when the SZAs are comparable. While this difference is within the reported errors of the two measured columns, the total columns observed from the ground are systematically 16–25% smaller than the total columns observed by GOME for SZAs between 80° and 88°, the difference increasing with decreasing SZA. Similar behavior is observed if only measurements within a 50 km radius of Arrival Heights are used, ruling out that horizontal inhomogeneities and the large GOME pixel are the main reason for the observed discrepancy. The equatorial offset of 4×10^{13} molecules cm^{-2} for the slant column used is an important factor in the total column retrieval from GOME. Decreasing the offset will decrease GOME BrO columns everywhere, but as it is applied to the slant columns, the effect is largest at high sun. The smallest air mass factor for the time series shown is about 4 which implies that the maximum effect of the equatorial offset is 1×10^{13} molecules cm^{-2}. Thus even the assumption of 0×10^{13} molecules cm^{-2} BrO over the equator (which hardly is a sensible assumption) could only explain 1×10^{13} molecules cm^{-2} of the observed difference seen in Figure 4.

[43] The mean ground-based 80° sunrise stratospheric column over all measurement days was $2.1 \pm 0.5 \times 10^{13}$ molecules cm^{-2} for the column integration above 15 km and the mean sunrise 84° stratospheric column above 15 km was $2.2 \pm 0.4 \times 10^{13}$ molecules cm^{-2}. The SCIAMACHY Limb BrO column above 15 km retrieved by *Sinnhuber et al.* [2005] for Arrival Heights for 18–27 September 2002 (SZA 83–86°) was $1.9 \pm 0.5 \times 10^{13}$ molecules cm^{-2}, slightly lower, but still in agreement with the ground-based stratospheric columns. Also using SCIAMACHY Limb data, *Sioris et al.* [2006] retrieve a BrO column of $2.9 \pm 0.3 \times 10^{13}$ molecules cm^{-2} above 15 km. This value is the mean stratospheric column above 15 km from overpasses on 8 of the 9 sunrise measurement days (refer to Figure 3, top plot) within 4° latitude and 12° longitude of Arrival Heights (C. E. Sioris, personal communication, 2006). The SZA of the SCIAMACHY overpasses used for this average ranged from to 75° to 89°. The SCIAMACHY retrieval of *Sioris et al.* [2006] is larger (at the 1σ level) than the ground-based stratospheric column observations at 80° and 84° above 15 km.

4.2. Tropospheric Columns

[44] The measured variance weighted mean background tropospheric column over all days excluding the high tropospheric BrO days was $0.3 \pm 0.3 \times 10^{13}$ molecules cm^{-2}. This is equivalent to 0.2 ± 0.2 ppt if the BrO is assumed to be well mixed throughout the troposphere. The retrieved tropospheric column for the high-BrO case of $1.8 \pm 0.1 \times 10^{13}$ molecules cm^{-2} was almost a third of the total column. If this tropospheric BrO is assumed to all be located and well mixed in the lowermost 0.5 km boundary layer, consistent with a ''bromine explosion'' event, it corresponds to a mixing ratio of about 12 ppt.

[45] A mean tropopause height of 8.8 km from ozonesondes was used for the derivation of the tropospheric columns. However, the tropopause was highly variable over the measurement period because of the perturbed stratosphere ranging from 7 km to 10 km. The mean tropospheric columns retrieved for 80° sunrise for tropopause heights of 7, 8.8 and 10 km as well as for 15 km (enabling comparison with *Sinnhuber et al.* [2005]; see below) are given in Table 2. The effect on the tropospheric column derived for different tropopause heights 7–10 km is within the variability of the observed columns. The column below 15 km at this polar latitude does include the lowermost stratosphere thus is significantly higher.

[46] A more significant impact on the tropospheric columns presented here is the influence of the a priori (as Table 1 shows for the 80° tropospheric column 0.5 degrees of freedom). Table 2 shows that doubling the a priori everywhere increases the 80° columns by 0.2×10^{13} molecules cm^{-2}, with the overall mean tropospheric quantity increasing from 0.33 to 0.46×10^{13} molecules cm^{-2} (for 80° sunrise the total column essentially increases by 0.16, and the stratospheric column decreases by 0.05). The 80° tropospheric columns are most sensitive to the a priori, thus Table 2 is illustrative of the maximal a priori impact. Tripling the a priori column leads only to a 75% increase in the mean tropospheric columns, and this is still within their given uncertainties. This gives us confidence that the choice of a priori used here does not lead us

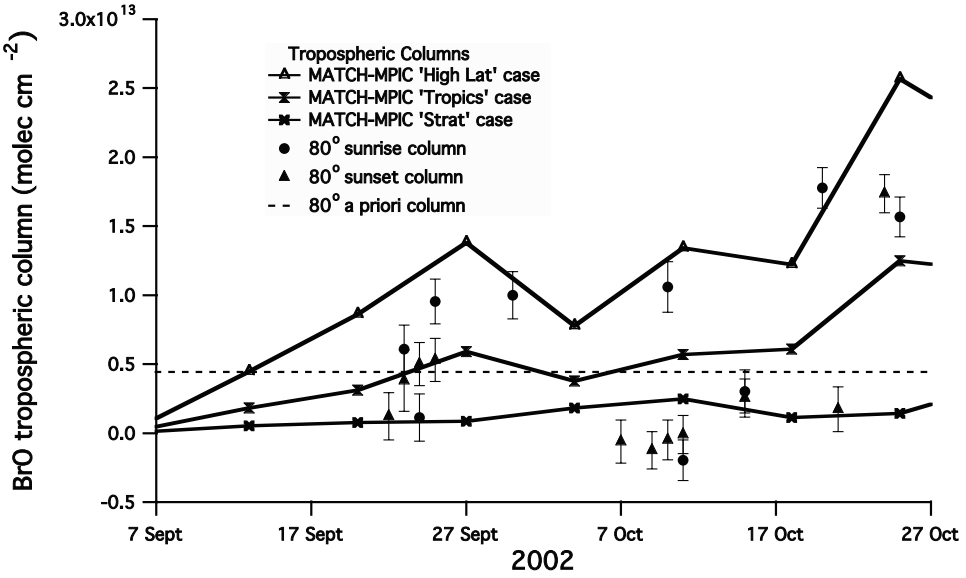

Figure 5. Tropospheric column comparison between ground-based 80° sunrise (solid circles) and 80° sunset (solid triangles) observations and MATCH-MPIC model daytime average calculated tropospheric columns (solid lines). Three MATCH-MPIC scenarios are presented. The MATCH-MPIC "strat" case is run with only downward transport of inorganic bromine from the stratosphere and decomposition of CH_3Br. The MATCH-MPIC "tropics" case (hourglasses) is run with an additional tropospheric bromine source which decreases with latitude. The "high lat" case (triangles) allows for the additional transport of air from "bromine explosion" events. For details on source scenarios, refer to *von Glasow et al.* [2004]. Also displayed (dashed line) is the tropospheric a priori column used for all 80° column retrievals.

to significantly underestimate the mean tropospheric column (extending the upper uncertainty bound only to $+0.7 \times 10^{13}$ molecules cm^{-2}).

[47] The Arrival Heights sunrise tropospheric columns are higher than the sunset columns. The diurnal variation of the retrieved sunrise tropospheric columns is stronger than the diurnal variation for retrieved sunset columns. The main source of tropospheric BrO is the breakdown of organic precursors and the photolysis of Br_2 and BrCl (the reaction of Br with O_3 occurs almost instantaneously and all the time) where the main sink is reaction with HO_2, which is only present later in the morning and gets weaker sooner than BrO (due to absorbing at shorter wavelengths) resulting in BrO maxima in the morning and late afternoon and a local minimum around noon [*von Glasow et al.*, 2002]. If high concentrations of NO_2 are present, with its diurnal variation a lot smaller than that of HO_2, this becomes the main sink for BrO and there is no midday dip. In the southern hemisphere there is little NO_x in the free troposphere. Therefore it is expected that BrO will have a stronger morning and a weaker evening peak, which is indeed the case in the MATCH-MPIC calculations and the retrieved columns. The columns retrieved from the ground-based measurements and the tropospheric columns calculated from different source scenarios from MATCH-MPIC are displayed in Figure 5. The MATCH-MPIC sunlit weekly average tropospheric columns are calculated for the different scenarios representative of different potential sources of tropospheric bromine (see section 3.2 above and *von Glasow et al.* [2004] for details).

[48] Given the very different spatial and temporal coverages between measurements and model, and with the consideration that the reanalysis data used for the model dynamics was from 1998, the comparison between the ground-based spectral point measurements and the weekly averaged model results can only be used as an indicator for which source scenario is reproducing the observations best in a semiquantitative way. This comparison shows that the sunrise measurements made at Arrival Heights are often consistent with the source scenarios "tropics" and "high lat." The scenario "strat" is usually lower than the sunrise measurements, pointing to the need for sources other than downward transport of inorganic bromine from the stratosphere (with $Br_y \sim 15$ ppt) and decomposition of CH_3Br to explain the measured tropospheric sunrise BrO columns. In contrast the sunset columns are lower and more consistent with the scenario "strat."

[49] Figure 6 displays the distribution of all of the tropospheric column retrievals (80°, 84° and 88° sunrise and sunset). Despite the large variability seen in Figure 5, the distribution is approximately normal about a mean of 0.3×10^{13} molecules cm^{-2} and standard deviation of 0.3×10^{13} molecules cm^{-2} for all of the columns excluding the high-BrO days. As Table 2 shows this number is somewhat sensitive to the a priori assumption, however a very high a priori tropospheric profile assumption with a peak of 3×10^{13} molecules cm^{-2} (similar in magnitude to the stratospheric BrO peak) results only in a slightly higher mean value of $0.6 \pm 0.4 \times 10^{13}$ molecules cm^{-2} for the background tropospheric BrO column. This background is consistent with, but slightly higher than, the tropospheric columns observed at Lauder of $0.2 \pm 0.2 \times 10^{13}$ molecules cm^{-2} [*Schofield et al.*, 2004a].

[50] The tropospheric columns for the high-BrO 24 October sunset and 25 October sunrise are displayed in Figure 6 with a mean tropospheric column of 1.8×10^{13}

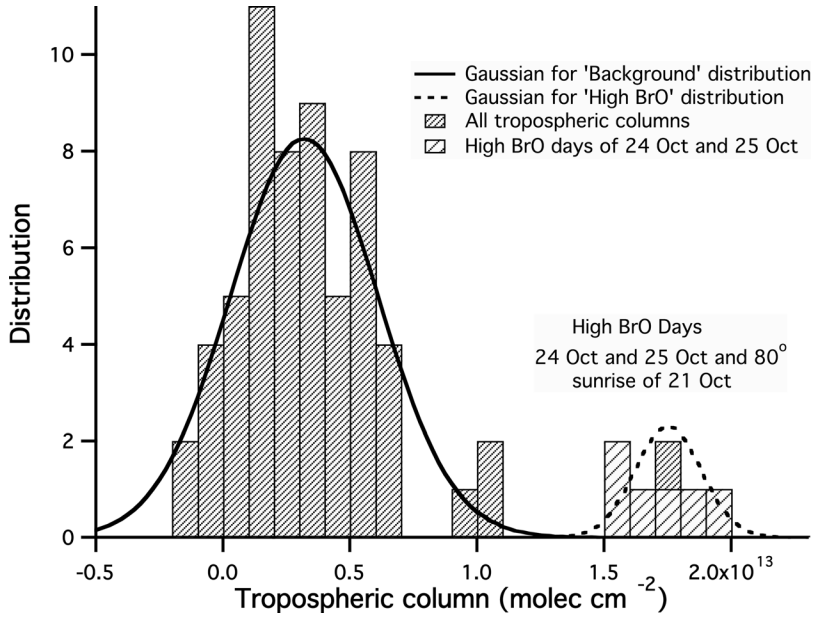

Figure 6. Distribution of all of the tropospheric column retrievals. The high tropospheric BrO events (24 and 25 October) have a significantly different distribution ($1.8 \pm 0.1 \times 10^{13}$ molecules cm^{-2}) compared to all the other tropospheric column retrievals ($0.3 \pm 0.3 \times 10^{13}$ molecules cm^{-2}).

molecules cm^{-2} and standard deviation of 0.1×10^{13} molecules cm^{-2}, statistically significantly different from the background days. The boundary layer BrO enhancement was also observed in GOME data on 24 October, where BrO columns increased by 2.5×10^{13} molecules cm^{-2} compared to the previous day, in good temporal agreement with the ground-based measurements. As the AMF used for the GOME analysis does not include a boundary layer enhancement, the BrO GOME column will be overestimated here.

[51] *Harder et al.* [1998] intercompare balloons with ground-based DOAS and GOME measurements for Kiruna (67.9°N, 21.1°E) in spring. Their study concludes a ubiquitous free tropospheric BrO amount of 1–2 ppt is required to explain the differences seen between the total columns of the ground-based and GOME observations and the stratospheric columns of the balloons. A similar intercomparison of *Van Roozendael et al.* [2002] found a tropospheric background of $1-3 \times 10^{13}$ molecules cm^{-2} extending over middle to high latitudes. Given the different locations and times of these studies comparison with the Arrival Heights study presented here is limited. Our high-BrO tropospheric columns are consistent, but the ubiquitous background BrO column that we observe is lower.

[52] *Richter et al.* [2002] performed a study involving correlation with O_4 SCDs to indicate tropospheric paths. This study found the GOME BrO column to be consistent with 0.5–2.0 ppt in the free troposphere over the remote equatorial Pacific in line with the studies of *Van Roozendael et al.* [2002] and *Harder et al.* [1998]. This is similar to our high tropospheric BrO columns (24–25 October), which have a mixing ratio of 1.1 ± 0.2 ppt if the column is assumed to be ubiquitous throughout the troposphere (tropopause of 8.8 km). However, our background mixing ratio is much lower than this at 0.2 ± 0.2 ppt (0.4 ± 0.3 ppt if 3× the a priori tropospheric profiles are assumed).

[53] The recent SCIAMACHY Nadir-Limb comparison of *Sinnhuber et al.* [2005] for 18–27 September 2002 infers a column below 15 km of $\sim 3 \times 10^{13}$ molecules cm^{-2} for high southern latitudes. The SZAs at Arrival Heights for this period decrease from 82° to 78° for the 1030 local time SCIAMACHY overpass. This is significantly higher than the integrated column up to 15 km for sunrise 80° profiles retrieved in this work of $1.7 \pm 0.9 \times 10^{13}$ molecules cm^{-2} (see Table 2). Even if the tropospheric a priori profiles 3× that shown in Figure 1 are assumed then this value is only $1.9 \pm 0.9 \times 10^{13}$ molecules cm^{-2}. The 80° column integration above 15 km of $2.1 \pm 0.5 \times 10^{13}$ molecules cm^{-2} for the ground-based observations is in good agreement with the Limb column observed by *Sinnhuber et al.* [2005] of $1.9 \pm 0.5 \times 10^{13}$ molecules cm^{-2}. Thus the discrepancy lies in the total column seen in the Nadir of $\sim 5 \times 10^{13}$ molecules cm^{-2} (in good agreement with the GOME Nadir columns, see Figure 4) compared to the total column observed here of $3.8 \pm 1.0 \times 10^{13}$ molecules cm^{-2} for 80° SZA.

[54] A recent modeling study by *Yang et al.* [2005] describes the tropospheric BrO source from bromocarbons and sea salt aerosols and removal by wet and dry deposition, in contrast to the different source scenario cases examined in the study of *von Glasow et al.* [2004] (shown in Figure 5). The simulated monthly mean tropospheric column of BrO near Arrival Heights for September and October 2002 was 0.83 and 0.41×10^{13} molecules cm^{-2}, respectively, with corresponding tropopause heights of 7.8 and 6.8 km (X. Yang, personal communication, 2006). The height of tropopause represents the averaged height of 2 PUV over Arrival Heights. Comparison with the retrieved columns here is complicated by the temporal sampling of the model (similar issues exist with the Match-MPIC comparison). The modeled tropospheric column values represent tropospheric column means between 0900 and

1500 horizontally interpolated to Arrival Heights, whereas the observations reported here include times outside this range (i.e., on 25 October 80° was at 0600 and 1900), and do not sample noon. With this caveat, the variance weighted mean tropospheric background columns over all tropospheric column retrievals (80°, 84° and 88° sunrise and sunset, tropopause heights consistent with those given above) were $0.37 \pm 0.21 \times 10^{13}$ molecules cm^{-2} and $0.21 \pm 0.30 \times 10^{13}$ molecules cm^{-2} for September and October, respectively. So while the mean decrease in columns from September to October is seen in both the observed and modeled tropospheric columns, the observed columns are approximately half those simulated by the modeling study of *Yang et al.* [2005]. A valuable future extension to the tropospheric column comparisons presented here (Match-MPIC in Figure 5 and X. Yang, personal communication, 2006) would be a comparison involving the diurnal variation of the modeled and observed tropospheric columns improving upon the temporal comparison.

5. Conclusions

[55] Tropospheric and stratospheric BrO columns were derived in this work by combining direct sun and zenith sky ground-based UV-visible spectroscopic measurements. The stratosphere over Arrival Heights, Antarctica in 2002 was highly variable because of the unprecedented southern hemispheric stratospheric warming resulting in a polar vortex split and reduced ozone loss relative to recent years.

[56] The ground-based measured stratospheric BrO columns were compared with SLIMCAT model columns. The BrO column observations from the ground are consistent with a SLIMCAT stratospheric Br_y loading of 21.2 ppt at 20 km. This is in line with recent estimates [*Sinnhuber et al.*, 2002; *Salawitch et al.*, 2005] but at the higher limit of 18.0 ± 3.0 ppt of *Sinnhuber et al.* [2005]. As such our stratospheric column observations are consistent with an additional 6 ± 3 ppt Br_y from short-lived sources included within the SLIMCAT simulations (the uncertainty given here is based on the observation-model agreement). As this comparison is conducted with CH_3Br as a surrogate for all bromine source gases within SLIMCAT, including the short-lived species, this should be viewed as a high limit (short-lived bromine species will result in less Br_y being required to agree with the BrO observations). The SLIMCAT model does not capture the observed decrease in the stratospheric BrO column for the vortex split on 21 September probably because of the coarser model resolution relative to the localized ground-based measurements. The return of the vortex air on 12 October resulted in little change in the stratospheric BrO columns, with both observations and SLIMCAT model results in good agreement for this extravortex to vortex air mass transition.

[57] The diurnal variation of the stratospheric BrO columns from 80° to 84° to 88° was retrieved from the ground-based observations. The increase in the stratospheric BrO column at sunrise from 88° to 80° seen in the observed columns is in good agreement with the diurnal change predicted by SLIMCAT. The sunset BrO stratospheric column observations showed little decrease from 80° to 88°, whereas the SLIMCAT model predicted a decrease symmetric to the increase seen at sunrise. The observed sunrise stratospheric columns are larger than the sunset columns ($3.1 \pm 0.6 \times 10^{13}$ molecules cm^{-2} compared to $2.6 \pm 0.4 \times 10^{13}$ molecules cm^{-2} for sunrise and sunset at 80°, respectively). The SLIMCAT model sunrise columns were also larger than the sunset columns, consistent with enhanced release of bromine from the nighttime reservoir BrCl (relative to HOBr) at colder temperatures.

[58] The tropospheric columns observed from the ground were compared with those calculated by the MATCH-MPIC model. The observed tropospheric sunrise columns were higher than the sunset columns, consistent with a strong diurnal variation in a clean remote site with low NO_x. The sunrise tropospheric BrO columns require an additional tropospheric source other than downward transport of inorganic bromine from the stratosphere and decomposition of CH_3Br to be explained. There is high variability in the retrieved tropospheric column retrievals; excluding the high-BrO days these columns are consistent with $0.3 \pm 0.3 \times 10^{13}$ molecules cm^{-2} (0.2 ± 0.2 ppt for a well-mixed troposphere). This low tropospheric "background" column is consistent with the column of 0.2 ± 0.3 ppt observed at Lauder, (45°S, 170°E) [*Schofield et al.*, 2004b], but at the lower end of the ~0.5–2.0 ppt estimates that have been inferred from ground-based observations, balloon observations, space observations and chemical model intercomparisons [*Harder et al.*, 1998; *Van Roozendael et al.*, 2002; *Richter et al.*, 2002; *Sinnhuber et al.*, 2005]. This discrepancy is consistent with the differences in the total BrO column observations, the cause of which remains unresolved. A statistically significantly high tropospheric "BrO explosion" event was observed with a tropospheric BrO column of $1.8 \pm 0.1 \times 10^{13}$ molecules cm^{-2}, this is equivalent to 12 ppt if it is assumed to be contained within a well-mixed 0.5 km boundary layer, consistent with BrO concentrations previously observed from the ground in the Arctic and Antarctic [*Tuckermann et al.*, 1997; *Kreher et al.*, 1997].

[59] The total BrO columns observed at the ground were compared with the GOME overpass measurements. This comparison was complicated by the differing SZAs and days of the respective measurements. The total BrO columns seen from the ground were consistently 16–25% lower than the GOME columns for SZAs between 80° and 88°.

[60] **Acknowledgments.** SAGE II NO_2 profiles were supplied by the NASA Langley Research Center (NASA-LaRC) and the NASA Langley Radiation and Aerosols Branch, 2002. The ozonesonde and aerosol profile data used in this publication were obtained as part of the Network for the Detection of Stratospheric Change (NDSC) (http://www.ndsc.ncep.noaa.gov), now the Network for the Detection of Atmospheric Composition Change (NDACC). In particular, we thank Chris Kroger and Paola Massoli. We thank Xin Yang, Christopher Sioris, and Björn-Martin Sinnhuber for kindly supplying the most comparable data for comparison with the work in this paper. R.S. wishes to thank the Foundation for Research Science and Technology Bright Future Fellowship scheme for providing funding. This work was also funded in part by the Foundation for Research in Science and Technology, program C01X0204. The authors wish to thank Antarctica, New Zealand, and the staff of Scott Base, Antarctica, for their help and support during the extended visit when this work was carried out.

References

Aliwell, S. R., et al. (2002), Analysis for BrO in zenith-sky spectra: An intercomparison exercise for analysis improvement, *J. Geophys. Res.*, *107*(D14), 4199, doi:10.1029/2001JD000329.

Allen, D. R., R. M. Bevilacqua, G. E. Nedoluha, C. E. Randall, and G. L. Manney (2003), Unusual stratospheric transport and mixing during the 2002 Antarctic winter, *Geophys. Res. Lett.*, *30*(12), 1599, doi:10.1029/2003GL017117.

Avallone, L. M., and D. W. Toohey (2001), Tests of halogen photochemistry using in situ measurements of ClO and BrO in the lower polar stratosphere, *J. Geophys. Res.*, *106*, 10,411–10,421.

Barrie, L. A., J. W. Bottenheim, R. C. Schnell, P. J. Crutzen, and R. A. Rasmussen (1988), Ozone destruction and photochemical reactions at polar sunrise in the lower Arctic atmosphere, *Nature*, *334*, 138–141.

Bottenheim, J. W., L. A. Barrie, E. Atlas, L. E. Heidt, H. Niki, R. A. Rasmussen, and P. B. Shepson (1990), Depletion of lower tropospheric ozone during Arctic spring: The Polar Sunrise Experiment 1988, *J. Geophys. Res.*, *95*, 18,555–18,568.

Brewer, A., C. T. McElroy, and J. Kerr (1973), Nitrogen dioxide concentration in the atmosphere, *Nature*, *246*, 129–133.

Burrows, J., et al. (1999), The Global Ozone Monitoring Experiment (GOME): Mission concept and first scientific results, *J. Atmos. Sci.*, *56*, 151–175.

Chipperfield, M. (1999), Multiannual simulation with a three-dimensional chemical transport model, *J. Geophys. Res.*, *104*, 1781–1805.

Chipperfield, M. (2006), New version of the TOMCAT/SLIMCAT off-line chemical transport model: Intercomparison of stratospheric tracer experiments, *Q. J. R. Meteorol. Soc.*, *132*, 1179–1204.

Danilin, M. Y., N. D. Sze, M. K. W. Ko, J. M. Rodriguez, and M. J. Prather (1996), Bromine-chlorine coupling in the Antarctic ozone hole, *Geophys. Res. Lett.*, *23*, 153–156.

Fish, D. J., and R. L. Jones (1995), Rotational Raman-scattering and the Ring effect in zenith-sky spectra, *Geophys. Res. Lett.*, *22*, 811–814.

Fish, D. J., R. L. Jones, and E. K. Strong (1995), Midlatitude observations of the diurnal variation of stratospheric BrO, *J. Geophys. Res.*, *100*, 18,863–18,871.

Fitzenberger, R., H. Bösch, C. Camy-Peyret, M. P. Chipperfield, H. Harder, U. Platt, B. M. Sinnhuber, T. Wagner, and K. Pfeilsticker (2000), First profile measurements of tropospheric BrO, *Geophys. Res. Lett.*, *27*, 2921–2924.

Frieß, U., K. Kreher, P. V. Johnston, and U. Platt (2005), Ground-based DOAS measurements of stratospheric trace gases at two Antarctic stations during the 2002 ozone hole period, *J. Atmos. Sci.*, *62*, 765–777.

Greenblatt, G. D., J. J. Orlando, J. B. Burkholder, and A. R. Ravishankara (1990), Absorption measurements of oxygen between 300 and 1140 nm, *J. Geophys. Res.*, *95*, 18,577–18,582.

Harder, H., et al. (1998), Stratospheric BrO profiles measured at different latitudes and seasons: Atmospheric observations, *Geophys. Res. Lett.*, *25*, 3843–3846.

Harder, J. W., J. W. Brault, P. V. Johnston, and G. H. Mount (1997), Temperature dependent NO_2 cross sections at high spectral resolution, *J. Geophys. Res.*, *102*, 3861–3879.

Heath, D. F., A. J. Krüger, H. A. Röder, and B. D. Henderson (1975), Solar backscatter ultraviolet and total ozone mapping spectrometer (SBUV-TOMS) for Nimbus G, *Opt. Eng.*, *14*, 323–331.

Hendrick, F., et al. (2004), Retrieval of nitrogen dioxide stratospheric profiles from ground-based zenith-sky UV-visible observations: Validation of the technique through correlative comparisons, *Atmos. Chem. Phys.*, *4*, 2091–2106.

Hendrick, F., et al. (2006), Intercomparison exercise between different radiative transfer models used for the interpretation of ground-based zenith-sky and multi-axis DOAS observations, *Atmos. Chem. Phys.*, *6*, 93–108.

Hönninger, G., and U. Platt (2002), Observations of BrO and its vertical distribution during surface ozone depletion at Alert, *Atmos. Environ.*, *36*, 2481–2489.

Hoppel, K., R. Bevilacqua, D. Allen, G. Nedoluha, and C. Randall (2003), POAM III observations of the anomalous 2002 Antarctic ozone hole, *Geophys. Res. Lett.*, *30*(7), 1394, doi:10.1029/2003GL016899.

Kaleschke, L., et al. (2004), Frost flowers on sea ice as a source of sea salt and their influence on tropospheric halogen chemistry, *Geophys. Res. Lett.*, *31*, L16114, doi:10.1029/2004GL020655.

Kreher, K., P. V. Johnston, S. W. Wood, B. Nardi, and U. Platt (1997), Ground-based measurements of tropospheric and stratospheric BrO at Arrival Heights, Antarctica, *Geophys. Res. Lett.*, *24*, 3021–3024.

Kromminga, H., J. Orphal, P. Spietz, S. Voigt, and J. P. Burrows (2003), New measurements of OClO absorption cross sections in the 325–435 nm and their temperature dependence between 213–293 K, *J. Photochem. Photobiol. A*, *157*, 149–160.

Lee, A. M., R. L. Jones, I. Kilbane-Dawe, and J. A. Pyle (2002), Diagnosing ozone loss in the extratropical lower stratosphere, *J. Geophys. Res.*, *107*(D11), 4110, doi:10.1029/2001JD000538.

Mateer, C. L., and H. U. Duetsch (1964), Uniform evaluation of Umkehr observations from the World Ozone Network, part I, Proposed standard evaluation technique, report, Natl. Cent. for Atmos. Res., Boulder, Colo.

McKenzie, R., P. Johnston, C. T. McElroy, J. Kerr, and S. Solomon (1991), Altitude distributions of stratospheric constituents from ground-based measurements at twilight, *J. Geophys. Res.*, *96*, 15,499–15,511.

Meller, R., and G. K. Moortgat (2000), Temperature dependence of the absorption cross sections of formaldehyde between 223 and 323 K in the wavelength range 225–375 nm, *J. Geophys. Res.*, *105*, 7089–7101.

Miller, H. L., A. Weaver, R. W. Sanders, K. Arpag, and S. Solomon (1997), Measurements of Arctic sunrise surface ozone depletion events at Kangerlussuaq, Greenland (67 degrees N, to 51 degrees W), *Tellus, Ser. B*, *49*, 496–509.

Noxon, J. (1975), Nitrogen dioxide in the stratosphere and troposphere measured by ground-based absorption spectroscopy, *Science*, *189*, 547–549.

Oltmans, S. J., et al. (1998), Trends of ozone in the troposphere, *Geophys. Res. Lett.*, *25*, 139–142.

Petropavlovskikh, I., P. K. Bhartia, and J. DeLuisi (2005), New Umkehr ozone profile retrieval algorithm optimized for climatological studies, *Geophys. Res. Lett.*, *32*, L16808, doi:10.1029/2005GL023323.

Pfeilsticker, K., et al. (2000), Lower stratospheric organic and inorganic bromine budget for the Arctic winter 1998/99, *Geophys. Res. Lett.*, *27*, 3305–3308.

Platt, U. (1994), Differential Optical Absorbtion Spectroscopy (DOAS), in *Air Monitoring By Spectroscopic Techniques*, *Chem. Anal. Ser. Monogr. Anal. Chem. Appl.*, vol. 127, edited by M. W. Sigrist, pp. 27–76, John Wiley, Hoboken, N. J.

Preston, K. E. (1995), The retrieval of NO_2 vertical profiles from ground-based twilight UV-visible absorption measurements, Ph.D. thesis, Univ. of Cambridge, Cambridge, U. K.

Preston, K. E., R. L. Jones, and H. K. Roscoe (1997), Retrieval of NO_2 vertical profiles from ground-based UV-visible measurements: Method and validation, *J. Geophys. Res.*, *102*, 19,089–19,097.

Ramanathan, K. R., and J. V. Dave (1957), The calculation of the vertical distribution of ozone by the Gotz Umkehr Effect (Method b), *Ann. Int. Geophys. Year*, *V*, 23–45.

Richter, A., F. Wittrock, M. Eisinger, and J. P. Burrows (1998), GOME observations of tropospheric BrO in Northern Hemispheric spring and summer 1997, *Geophys. Res. Lett.*, *25*, 2683–2686.

Richter, A., F. Wittrock, A. Ladstätter-Weienmayer, and J. P. Burrows (2002), GOME measurements of stratospheric and tropospheric BrO, *Adv. Space Res.*, *29*, 1667–1672.

Rodgers, C. D. (2000), *Inverse Methods for Atmospheric Sounding: Theory and Practice*, *Ser. Atmos. Oceanic Planet. Phys.*, vol. 2, 1st ed., World Sci., Hackensack, N. J.

Salawitch, R. J., D. K. Weisenstein, L. J. Kovalenko, C. E. Sioris, P. O. Wennberg, K. Chance, M. K. W. Ko, and C. A. McLinden (2005), Sensitivity of ozone to bromine in the lower stratosphere, *Geophys. Res. Lett.*, *32*, L05811, doi:10.1029/2004GL021504.

Sander, S. P., et al. (2003), Chemical kinetic and photochemical data for use in stratospheric modeling, evaluation no. 14, *Tech. Rep. 02-25*, Jet Propul. Lab., Pasadena, Calif.

Schofield, R. (2003), The vertical distribution of atmospheric BrO from ground-based measurements, Ph.D. thesis, Univ. of Auckland, Auckland, N. Z.

Schofield, R., B. J. Connor, K. Kreher, P. V. Johnston, and C. D. Rodgers (2004a), The retrieval of profile and chemical information from ground-based UV-visible spectroscopic measurements, *J. Quant. Spectrosc. Radiat. Transfer*, *86*, 115–131.

Schofield, R., K. Kreher, B. J. Connor, P. V. Johnston, A. Thomas, D. Shooter, M. P. Chipperfield, C. D. Rodgers, and G. H. Mount (2004b), Retrieved tropospheric and stratospheric BrO columns over Lauder, New Zealand, *J. Geophys. Res.*, *109*, D14304, doi:10.1029/2003JD004463.

Schroeder, W. H., and J. Munthe (1998), Atmospheric mercury—An overview, *Atmos. Environ.*, *32*, 809–822.

Simpson, W. R., L. Alvarez-Aviles, T. A. Douglas, M. Sturm, and F. Domine (2005), Halogens in the coastal snow pack near Barrow, Alaska: Evidence for active bromine air-snow chemistry during springtime, *Geophys. Res. Lett.*, *32*, L04811, doi:10.1029/2004GL021748.

Sinnhuber, B.-M., et al. (2002), Comparison of measurements and model calculations of stratospheric bromine monoxide, *J. Geophys. Res.*, *107*(D19), 4398, doi:10.1029/2001JD000940.

Sinnhuber, B.-M., et al. (2005), Global observations of stratospheric bromine monoxide from SCIAMACHY, *Geophys. Res. Lett.*, *32*, L20810, doi:10.1029/2005GL023839.

Sinreich, R., U. Frieß, T. Wagner, and U. Platt (2005), Multi axis differential optical absorption spectroscopy (MAX-DOAS) of gas and aerosol distributions, *Faraday Discuss.*, *130*, 153–164.

Sioris, C. E., et al. (2006), Latitudinal and vertical distribution of bromine monoxide in the lower stratosphere from Scanning Imaging Absorption Spectrometer for Atmospheric Chartography limb scattering measurements, *J. Geophys. Res.*, *111*, D14301, doi:10.1029/2005JD006479.

Solberg, S., N. Schmidbauer, A. Semb, F. Stordal, and O. Hov (1996), Boundary-layer ozone depletion as seen in the Norwegian Arctic in spring, *J. Atmos. Chem.*, *23*, 301–332.

Solomon, S. (1999), Stratospheric ozone depletion: A review of concepts and history, *Rev. Geophys.*, *37*, 275–316.

Solomon, S., A. L. Schmeltekopf, and R. W. Sanders (1987), On the interpretation of zenith sky absorption measurements, *J. Geophys. Res.*, *92*, 8311–8319.

Tang, T., and J. C. McConnell (1996), Autocatalytic release of bromine from Arctic snow pack during polar sunrise, *Geophys. Res. Lett.*, *23*, 2633–2636.

Tuckermann, M., R. Ackermann, C. Golz, H. Lorenzenschmidt, T. Senne, J. Stutz, B. Trost, W. Unold, and U. Platt (1997), DOAS-observation of halogen radical-catalysed Arctic boundary layer ozone destruction during the ARCTOC-campaigns 1995 and 1996 in Ny-Alesund, Spitsbergen, *Tellus, Ser. B*, *49*, 533–555.

Van Roozendael, M., et al. (2002), Intercomparison of BrO measurements from ERS-2 GOME, ground-based and balloon platforms, *Adv. Space Res.*, *29*, 1661–1666.

Voigt, S., J. Orphal, K. Bogumil, and J. P. Burrows (2001), The temperature dependence (203–293 K) of the absorption cross sections of O_3 in the 230–850 nm region measured by Fourier-transform spectroscopy, *J. Photochem. Photobiol. A*, *143*, 1–9.

von Glasow, R., R. Sander, A. Bott, and P. J. Crutzen (2002), Modeling halogen chemistry in the marine boundary layer: 1. Cloud-free MBL, *J. Geophys. Res.*, *107*(D17), 4341, doi:10.1029/2001JD000942.

von Glasow, R., R. von Kuhlmann, M. Lawrence, U. Platt, and P. J. Crutzen (2004), Impact of reactive bromine chemistry in the troposphere, *Atmos. Chem. Phys.*, *4*, 2481–2497.

von Kuhlmann, R., M. G. Lawrence, P. J. Crutzen, and P. J. Rasch (2003), A model for studies of tropospheric ozone and nonmethane hydrocarbons: Model description and ozone results, *J. Geophys. Res.*, *108*(D9), 4294, doi:10.1029/2002JD002893.

Wagner, T., B. Dix, C. v. Friedeburg, U. Frieß, S. Sanghavi, R. Sinreich, and U. Platt (2004), MAX-DOAS O_4 measurements: A new technique to derive information on atmospheric aerosols—Principles and information content, *J. Geophys. Res.*, *109*, D22205, doi:10.1029/2004JD004904.

Wilmouth, D. M., T. F. Hanisco, N. M. Donahue, and J. G. Anderson (1999), Fourier transform ultraviolet spectroscopy of the $A(^2\Pi_{3/2}) \leftarrow X(^2\Pi_{3/2})$ transition of BrO, *J. Phys. Chem.*, *103*, 8935–8945.

World Meteorological Organization (WMO) (2003), Scientific assessment of ozone depletion: 2002, *Global Ozone Res. Monit. Proj. Rep. 47*, 498 pp., Geneva.

Yang, X., R. A. Cox, N. J. Warwick, J. A. Pyle, G. D. Carver, F. M. O'Connor, and N. H. Savage (2005), Tropospheric bromine chemistry and its impacts on ozone: A model study, *J. Geophys. Res.*, *110*, D23311, doi:10.1029/2005JD006244.

M. P. Chipperfield, Institute for Atmospheric Science, School of Earth and Environment, University of Leeds, LS2 9JT Leeds, UK.

B. J. Connor, K. Kreher, P. V. Johnston, A. Thomas, and S. Wood, National Institute of Water and Atmospheric Research, Private Bag 50061, Omakau 9182, Central Otago, New Zealand.

A. Richter, Institute of Environmental Physics, University of Bremen, Otto-Hahn-Allee 1, D-28359 Bremen, Germany.

C. D. Rodgers, Atmospheric, Oceanic and Planetary Physics, Department of Physics, University of Oxford, Parks Road, Oxford OX1 3PU, UK.

R. Schofield, Chemical Sciences Division, Earth Systems Research Laboratory, NOAA, 325 Broadway, Boulder, CO 80305, USA. (robyn.schofield@noaa.gov)

D. Shooter, School of Geography and Environmental Science, University of Auckland, Private Bag 92019, Auckland, New Zealand.

R. von Glasow, Institute of Environmental Physics, Univ. Heidelberg, Im Neuenheimer Feld 229, D-69120 Heidelberg, Germany.